12/05

TOOL FORCES DEVELOPED DURING FRICTION STIR WELDING

M. Melendez, W. Tang[+], C. Schmidt, J. C. McClure, A. C. Nunes*, L. E. Murr

Metallurgical and Materials Engineering Department
University of Texas at El Paso

[+]Mechanical Engineering Department,
University of South Carolina, Columbia, S.C.

*NASA Marshall Space Flight Center,
Huntsville, Alabama

ABSTRACT

This paper will describe a technique for measuring the various forces and the torque that exist on the Friction Stir Welding pin tool. Results for various plunge depths, weld speeds, rotational speed, and tool configurations will be presented. Welds made on 6061 aluminum with typical welding conditions require a downward force of 2800 lbs. (12.5 kN) a longitudinal force in the direction of motion of 300 lbs (1.33 kN), a transverse force in the ω x **v** direction of 30 lbs (135 N). Aluminum 2195 under typical weld conditions requires a downward force of 3100 lbs. (13.8 kN), a longitudinal force of 920 lbs. (4.1 kN), and a transverse force of 45 lbs. (200 N) in the ω x **v** direction.

INTRODUCTION

Friction stir welding (FSW), a remarkable modification of traditional friction welding, was invented in early 90's by The Welding Institute[1]. During Friction Stir Welding, the parts to be butt welded are clamped to a backing plate. A rapidly rotating cylindrical pin tool is then slowly plunged into the centerline of the joint until the

shoulder of the pin tool comes into contact with the work piece surface. Heating causes the material yield strength to decrease and, as the pin tool moves along the joint, material moves around the pin tool closing the joint behind the tool. As a solid state welding method, FSW can avoid all the welding defects caused by the melting and solidification in fusion welding and has more versatility than traditional friction welding which normally is limited to small axisymmetric parts. During the past decade Friction Stir Welding work has focused in the welding method itself[2, 3], microstructure of the welded joint[4-9], temperature distribution[10, 11], and material motion during welding [12-14]. The forces the pin tool experiences during the FSW process have been studied recently by Tang, *et. al*[17]; this paper reports force measurements made under somewhat different conditions than Tang so results are difficult to compare directly. Results are in general agreement, however. Phenomenological models are presented for the various forces.

EXPERIMENT

Experimental welds were performed on 0.25 in. (6.35 mm.) thick 6061-T6 and 2195-T6 aluminum alloys using the instrumented structure shown in Fig. 1 mounted on a 2.5 HP Gorton Master Mill. The vertical compliance of the mill was measured using a ring stress gauge and a dial indicator and was $5x10^{-6}$ inches/lb. ($2.8x10^{-5}$ mm/N) which is small enough to neglect in this study. Aluminum 6061 is a common Al-Mg-Si alloy and 2195 is a new lithium-containing alloy that is difficult to weld by fusion techniques. Mechanical properties of the alloys are unfortunately not well known at the high welding temperatures so the behavior of the two alloys is difficult to compare. The thermal conductivity of 2195 is much lower than that of 6061 (approximately 90W/m ^{o}K compared to 180 W/m ^{o}K)[18].

The upper plate of the structure is a thick steel plate (14×10×1in.) (35.5×25.4×2.54 cm.) supported by three steel beams. These beams were then fixed on a lower steel plate so that the whole structure can be attached to the table of the milling machine. The top and bottom surfaces of the channel iron beams were machined to be parallel to each other and perpendicular to the web of the beam. Points A and B immediately over the beams are high symmetry points, and stress measurements were made when the pin tool was over these points. Points A and B are two inches (5cm) from the beginning and end of the weld to minimize starting and ending temperature transients.

General purpose ¼ inch strain gauges (supplied by Measurement Systems, Inc.) were pasted on the beams as shown in Fig. 2. Although compensated for thermal expansion of steel, dummy gauges were located at points on the structure that were stress free but were at nearly same temperature as the measurement gauges. To verify that temperature variations did not effect the measurements, it was noted that all strains returned to the original values after a weld was completed. The strain gauges were connected to a computer through modules SCXI-1121, SCXI-1100 data acquisition boards manufactured by National Instruments; these modules are commonly used with strain gauges and include current or voltage excitation and internal Wheatstone bridge completion circuits. A program written by National Instruments in Labview programming language was used to record the strain data during the calibration tests and the actual welding process.

Bead-on-plate welds required the same forces as standard butt welds so most of the data reported here are from bead-on-plate welds. Friction stir welds were made under different weld conditions by varying plunge depth, tool rotational speed, welding speed,

tool geometry, and lead angle of the tool. The aluminum plates used in all welds had dimensions of 12×4×1/4 in. (30.4×10×.64 cm), and were clamped to the upper plate of the instrumented structure (fig. 1) by four clamps. The rotating tool was made from hardened O-1 tool steel; the tool shoulder was 0.75 in. (19.2 mm) in diameter and the pin or nib had a diameter 0.25 in. (6.35 mm) inches and was 0.23 in. (5.83 mm.) long with a standard ¼-20 thread. Unless noted, the rotation of the tool was in a counterclockwise direction such that the threads on the pin tool pushed material downward. The pin tool had a 1° lead angle.

The strain gauges are designated with two subscripts: the first referring to the beam where the gauge is pasted on (fig.1 top view) with subscript i, and the second subscript, j, refers to the particular gauge on that beam (fig. 2).

Strains were measured assuming that for a strain gauge on beam i and location j (fig. 1 and 2) the measured strain ε_{ij} can be expressed as,

$$\varepsilon_{ij} = \varepsilon_{ij}^{F_d} + \varepsilon_{ij}^{F_l} + \varepsilon_{ij}^{F_t} + \varepsilon_{ij}^{T} \qquad (1)$$

since strain, in any gauge, is caused by a combination of forces, where $\varepsilon_{ij}^{F_d}$ is the strain at ij caused by the downward force, $\varepsilon_{ij}^{F_l}$ is the strain at ij caused by the longitudinal force, $\varepsilon_{ij}^{F_t}$ is the strain caused by the transverse force, and ε_{ij}^{T} is the strain at ij caused by the torque.

To calculate the strain caused by the downward force, the strain of gauge 3-1 was measured when forces are applied by the pin tool at point A, $\varepsilon_{3\text{-}1}^{A}$, and at point B, $\varepsilon_{3\text{-}1}^{B}$,

$$\varepsilon_{3-1}^{B} - \varepsilon_{3-1}^{A} = (\varepsilon_{3-1}^{F_d} + \varepsilon_{3-1}^{Fl} + \varepsilon_{3-1}^{Ft} + \varepsilon_{3-1}^{T})^{B} - (\varepsilon_{3-1}^{F_d} + \varepsilon_{3-1}^{Fl} + \varepsilon_{3-1}^{Ft} + \varepsilon_{3-1}^{T})^{A} \qquad (2)$$

Note that strains on the left hand side are the actual experimentally measured strains when the pin tool was at either A or B on the structure. On the right hand side of the equation most of the terms cancel out by symmetry. For example, there is no effect of the transverse force on gauge 3-1 at point A since gauge 3-1 is located at beam 3 below point B, and $(\varepsilon_{3-1}^{F_t})^A = 0$. Furthermore, the longitudinal force does not depend on the position of the pin tool, so the strain caused by the longitudinal force is the same at A and B, and $(\varepsilon_{3-1}^{F_l})^A = (\varepsilon_{3-1}^{F_l})^B$. Finally, we are left with

$$\varepsilon_{3-1}^{F_d} = \varepsilon_{3-1}^{B} - \varepsilon_{3-1}^{A} \tag{3}$$

To determine the strain caused by the longitudinal force, the strain of gauges 1-2 and 2-3 when the pin tool is at point A, $\varepsilon_{1\text{-}2}{}^{A}$ and $\varepsilon_{2\text{-}3}{}^{A}$, were used. Again

$$\varepsilon_{1-2}^{A} - \varepsilon_{2-3}^{A} = (\varepsilon_{1-2}^{F_d} + \varepsilon_{1-2}^{F_l} + \varepsilon_{1-2}^{F_t} + \varepsilon_{1-2}^{T})^A - (\varepsilon_{2-3}^{F_d} + \varepsilon_{2-3}^{F_l} + \varepsilon_{2-3}^{F_t} + \varepsilon_{2-3}^{T})^A \tag{4}$$

From symmetry, and verified by testing, the strain on gauges 1-2, and 2-3, have the same magnitude and sign when a downward load was applied at point A; strain gauges 1-2 and 2-3 have same magnitude but opposite sign with a longitudinal load at A; strain gauges 1-2 and 2-3 have same sign and magnitude due to a transverse load at A; and strain gauges 1-2 and 2-3 also have same sign and magnitude due to a torque applied

$$\varepsilon_{1-2}^{F_d} = \varepsilon_{2-3}^{F_d}, \qquad \varepsilon_{1-2}^{F_l} = -\varepsilon_{2-3}^{F_l}, \qquad \varepsilon_{1-2}^{F_t} = \varepsilon_{2-3}^{F_t}, \qquad \varepsilon_{1-2}^{T} = \varepsilon_{2-3}^{T},$$

at point A.

Therefore, all the terms cancel out except the strains caused by the longitudinal force resulting in:

$$\varepsilon_{1-2}^{F_l} = \frac{\varepsilon_{1-2}^{A} - \varepsilon_{2-3}^{A}}{2} \tag{5}$$

For strain caused by the transverse force, the strain on gauges 1-2 and 2-2, ε^{A}_{1-2} and ε^{A}_{2-3}, at point A, were used,

$$\varepsilon^{A}_{1-2} - \varepsilon^{A}_{2-2} = (\varepsilon^{F_a}_{1-2} + \varepsilon^{F_t}_{1-2} + \varepsilon^{F_t}_{1-2} + \varepsilon^{T}_{1-2})^{A} - (\varepsilon^{F_a}_{2-2} + \varepsilon^{F_t}_{2-2} + \varepsilon^{F_t}_{2-2} + \varepsilon^{T}_{2-2})^{A} \quad (6)$$

From symmetry it can be noted that magnitudes and signs are equal for all the terms except the strains caused by the transverse force.

$$(\varepsilon^{F_a}_{1-2})^{A} = (\varepsilon^{F_a}_{2-2})^{A}, \qquad (\varepsilon^{F_t}_{1-2})^{A} = (\varepsilon^{F_t}_{2-2})^{A}, \qquad (\varepsilon^{F_t}_{1-2})^{A} = -(\varepsilon^{F_t}_{2-2})^{A}, \qquad (\varepsilon^{T}_{1-2})^{A} = (\varepsilon^{T}_{2-2})^{A},$$

Therefore,

$$\varepsilon^{F_t}_{2-2} = \frac{\varepsilon^{A}_{1-2} - \varepsilon^{A}_{2-2}}{2} + (\varepsilon^{T}_{1-2})^{A} \quad (7)$$

In equation (7), the strain caused by the transverse force can be obtained if the strain caused by the torque is known.

Pin tool torque was measured using the input power to the welder with an Esterline-Angus digital PMT-A power meter to measure the current, voltage, and phases of the three phase input electrical power to the milling machine during welding experiments. Motor electrical efficiency was estimated to be 80%, which is typical of similar motors and should be in error by no more than 5%.

The torque, T, during the welding process can be obtained from the electrical power measurements using

$T = \frac{P}{2\pi f}$, Where f is the rotational frequency and P is measured power. (8)

The symmetry and compliance of the weld fixture were determined by applying known weights and torques to studs located at points A and B. Longitudinal and transverse loads were applied to the test fixture by hanging weights using a fixed pulley

and wire attached to the studs as shown in Figure 3. A ring force gauge, manufactured by Morehouse Co., was used for the downward force calibration to measure the applied force to the instrumented structure and record strain readings. A digital torque wrench was used to apply torques to studs located at A and B. The response of the test fixture to the known applied loads was,

$$F_d = 19.3\times10^6\,\varepsilon_{3-1}^{F_d} \quad \text{lbs.} \tag{10}$$

$$F_l = 10\times10^6\,\varepsilon_{1-2}^{F_l} \quad \text{lbs.} \tag{11}$$

$$F_t = 3.0\times10^6\,\varepsilon_{2-2}^{F_t} \quad \text{lbs.} \tag{12}$$

The strains on the right hand sides can be determined from the experimentally measured strains (with superscripts A or B) from Eqs. 3, 5, 7. Equations (10), (11), and (12) are used to convert the measured strain to actual forces. With the strains and torque (determined electrically) measured during the welding process and the calibration test results above, the various forces and torque on the work piece can be obtained.

The size of the dynamically recrystallized zone around the pin tool was measured on polished sections of weld cut transverse to the weld direction. The samples were etched in Keller's reagent and measurements were made using a stage micrometer at 10x magnification.

RESULTS AND DISCUSSION

Effect of Plunge Depth.

Plunge depth is the distance the back of the pin tool shoulder is plunged or submerged into the material before and during the weld. Plunge depth was varied from

0.035 in. (0.89 mm.) to 0.050 in. (1.27 mm.) in increments of 0.005 in. (0.13 mm.) in these experiments, and the rotational velocity of the pin tool was constant at 800rpm. The pin tool was tilted back (lead angle) at 1° and the welding speed was 2mm/s. Appreciably more shallow plunge depths risk poor fusion and larger plunge depths leave excessive flash on the retreating side (the side of the weld in which the nib rotation and the nib traverse are in the same direction) of the weld.

Longitudinal Force

Longitudinal force is the force needed to push the pin tool along the faying surface during welding. As can be seen in Figure 4 the longitudinal force for 6061 increases with plunge depth. This increase is expected since the shoulder is deeper into the work piece and must move a greater volume of material. Longitudinal force increases linearly with plunge depth from 134lbs. (600 N) for a plunge of 0.035 in. (0.89 mm.). to 330 lbs. (1.5 kN) for a plunge depth of 0.050in. (1.27 mm.).

For an estimate on the size of the longitudinal force, one can consider the pin tool and material rotating with it as a conical indenter with base equal to the diameter of the recrystallized zone and height equal to the length of the pin tool that is pushed sideways through the work piece. No solution exists for such an indenter, but an upper limit on the force can be obtained if the pin tool is considered as a flat punch with cross sectional area equal to the frontal area of the cone formed by the pin tool and material rotating with it. Such a flat punch will require six times the yield stress of the work piece times the cross sectional area, to cause plastic deformation[15]. The yield strength of 6061 aluminum at the 450° C[8] welding temperature can be very roughly estimated by extrapolating data from the *Handbook of Aluminum*[16] to be 1.5 ksi. (10.3 MPa), and the estimated cross sectional

area is 0.031in ^{2}. To push such a rotational zone through this material will require about 285 lbs. (1.3 kN) in rough agreement with measured values.

Figure 4 shows a data point made with no lead angle (pin tool perpendicular to the work piece) and the longitudinal force increases due to a ridge of material, which builds up at the front of the shoulder rather than being rotated around and under the shoulder.

On the other hand, for aluminum 2195 the longitudinal force is much larger and decreases with plunge depth as observed in Figure 4. A longitudinal force of 1096 lbs. (4.9 kN) was obtained for a plunge depth of 0.035 in. (0.89 mm.), and 800 lbs. (3.6 kN) for a plunge of 0.050in. (1.27 mm.). Cross sections of welds on 2195 made at shallow and deep plunges showed a very different shaped recrystallized zone [19]. The deeper plunge had a more conical zone that flared out to the shoulder diameter. The shallow plunge sample had a nearly cylindrical shaped recrystallized zone. In the case of 6061 the recrystallized zone barely changes in size or shape as plunge depth is changed. It is not known why the two alloys behave so differently, but the different slope of the longitudinal force with plunge depth (negative for 2195 and positive for 6061) may be related to the very different shapes of the recrystallized zone that surrounds the pin tool in the two alloys.

Transverse Force

The transverse forces are much smaller than the longitudinal and downward forces. Since the transverse force depends on the difference of two strains which do not differ greatly, the measured values in Figure 4 may not be as accurate as the other forces.

Nevertheless, changing the direction of rotation of the pin tool did change the direction of the transverse force and showed a similar magnitude.

The probable origin of the transverse force is a mismatch of reactions between the front and back of the pin tool. It can be seen in Figure 5 that there is a greater reaction in the front of the pin tool because the temperature of aluminum is lower and the flow stress is higher than that at the back which has hotter and softer material. This mismatch of forces causes a transverse or sideways force on the work piece in the ω x **v** direction where ω is the rotational direction of the pin tool and **v** is the weld direction. The transverse force does not change greatly with plunge depth since most material is moved around the pin tool by the pin rather than the shoulder.

Downward Force

The downward force varies directly with plunge depth. Downward force increases with increasing plunge depth for both alloys as can be seen in Figure 6. Again considering the shoulder to be a flat punch that is pushed into the work piece, a downward force of three times the yield stress times the area of the shoulder or about 2000 lbs. (8.9 kN) would be expected for 6061 which is smaller than the observed 2000 (8.9 kN) to 3000 lbs. (13.3 kN) forces.

However, the pin tool is inclined by 1° and moving so there is an additional component due to the longitudinal force that pushes up (an analogy with skiing comes to mind) and must be overcome by an additional downward force to maintain a given plunge depth. This effect can be seen in Figure 6 which includes a point made without lead angle and shows a 300 lbs. (1.3 kN) reduction in downward force. A simple

A clear limitation of the simple punch model is that it assumes a uniform yield strength of the material and hence force (for shallow plunges) is independent of depth. This clearly is not the case with Friction Stir Welding. Presumably at greater plunges a greater force is needed because of a larger plastic zone that extends into material with a lower temperature and higher yield strength.

Effect of Tool Angular Velocity

Longitudinal Force

The longitudinal force showed an increase for both Al 6061 and Al 2195 when the tool rotational speed was increased (Figure 7). This may be caused by the larger volume of material in the dynamically recrystallized zone (DRZ) that the pin has to create while advancing. Fig. 8 shows the width of the dynamically recrystallized zone measured at mid thickness on weld cross sections as a function of rotational speed. It can be seen that the size of the dynamically recrystallized zone increases with rotational speed, which raises the effective frontal area that must be pushed through the work piece as the tool advances.

Transverse Force

The transverse force (see Fig. 7) remains small compared to other forces when rotational speed is changed. The alloy 2195 always produced a larger transverse force than 6061.

Downward Force

The downward force (Figure 9) decreases when increasing the rotational speed of the tool in FSW. This decrease may have two causes: 1) The temperature of the work piece increases with rotational speed so the material is softer and requires less downward

force at a given plunge depth and 2) a faster rotating pin tool removes material more quickly from under the shoulder so a given plunge depth is obtained with less downward force.

Effect of Welding Speed

Longitudinal Force

The longitudinal force increases with increasing weld speed as shown in Figure 10. This increase is expected because there are fewer revolutions of the pin tool per unit distance of travel and so material is more likely to be squeezed around the pin tool than to be rotated around the pin tool. In the limit of an extremely fast weld, the pin tool does not rotate at all and all material must be squeezed around the pin tool.

Transverse Force

Figure 10 also shows that the transverse force is small but shows a modest increase with weld speed for both alloys. Note that at higher weld speeds, heat has less time to diffuse ahead of the weld and there will be a greater difference in temperature between the front and back of the weld. As discussed above, this should produce a greater transverse force.

Downward Force

The downward force decreased as a function of welding speed for Al 6061 and increased for Al 2195 as seen in Figure 11. Due to the finite thermal diffusivity, higher weld speeds lead to cooler and stronger material ahead of the weld. Thus, a larger downward force is expected at higher weld speeds. This is the case for the low thermal conductivity of Al 2195. For the more conductive 6061 a smaller change with weld speed is expected, but it is not clear why the slope should be negative as seen in Fig. 11.

Microstructural changes with weld speed for the two alloys may be different, but more work needs to be performed to understand this behavior.

Tool Geometry

The effect of different shoulder geometries on the forces during FSW was observed by changing the diameter and configuration of the shoulder. A typical tool shoulder, such as the one used in this study, has a diameter of 0.75 in (1.9cm). and for this experiment the diameter was changed to 0.5 in. (1.3cm) and 1.0 in. (2.5cm). In addition, changes in the geometry of the shoulder, seen in Figure 12, were made by cutting flutes, and channels in the face of the shoulder to see force variations compared to a standard 0.75 in. (1.9cm) diameter, flat shoulder tool.

Longitudinal Force

From Figure 12 it can be observed that the longitudinal force increased for the welds with fluted shoulder tools. This increase in the longitudinal force is probably caused by the additional material that is stirred by the flutes and an effective increase in the cross sectional area of the pin tool as it is pushed through the work piece.

Transverse Force

The transverse force increased slightly with the fluted shoulders. This increase is caused by the severe stirring of the aluminum in contact with the shoulder causing a greater reaction between colder material in front and hotter material in the back of the pin tool. For the tool with channels in the shoulder there was a decrease in the transverse force due to less contact surface area between the work piece and the shoulder

Downward Force

As seen in the Figure, the downward force decreases from a value of approximately 2900 lbs. (12.9 kN), obtained with a standard tool, to 1600 lbs. (7.2 kN) for the fluted shoulder tools. This is believed to happen because the flutes gouge out material more effectively than the smooth shoulder and it is easier to plunge the tool into the gouged out work piece.

To determine the effect of shoulder diameter on weld forces, pin tools with shoulder diameters of .5 in. (1.3cm) and 1.0 in. (2.5cm) were machined and compared with the standard .75 in. (1.9cm) shoulder used for the other welds in this work. Results are shown in Figure 13 and 14 for aluminum 6061. The longitudinal, transverse and downward forces all increase with increasing shoulder diameter. The increase in the forces with increasing shoulder diameter can be attributed to greater contact area between the tool and the work piece causing greater reactions in all three directions.

Torque

The power needed to advance the pin tool during welds is negligible compared to the power consumed in rotating the pin tool. When the pin tool is stationary during initial plunge, the power increases until intimate contact between the shoulder and work piece is achieved. Once a final plunge depth is reached, the power until the pin tool is advanced when it again increases. Power remains nearly constant with pin tool rotational velocity indicating a decreasing torque.

Specific weld energy was measured using power readings versus welding speed. It can be seen in Figure 15 that energy per unit distance of weld decreases as the welding speed increases. This behavior is typical of all forms of welding because at high weld speeds, less heat "escapes" from the immediate vicinity of the heat source. The lower

thermal conductivity 2195 requires less work to weld since heat diffuses away from the weld zone more slowly.

It is interesting to compare the specific weld energy of Friction Stir Welds with that of fusion welds. For example, to weld .25 inch 6061 aluminum at 4mm/sec, (excluding electrical losses in the motor) approximately 670 J/mm of energy are required. This can be compared to Plasma Arc welding of similar aluminum which typically requires 140A and 31V for 1,080 J/mm.

In fusion welding it is common to distinguish between "arc efficiency" and "melting efficiency". Arc efficiency is the percentage of the electrical power that is actually transferred to the work piece and varies with the kind of welding (TIG, PAW, SMAW) but is typically around 50%. The equivalent power loss in Friction Stir Welding is loss in the spindle motor which for typical motors is around 20%. Melting efficiency is the percentage of this transferred power that goes into melting the work piece. For fusion welding melting efficiency is independent of the type of welding but varies with weld speed, work piece thermal diffusivity, and work piece thickness. Thick work pieces have low melting efficiency because heat is efficiently removed from the weld pool by the surrounding material. Friction stir welding, of course, does not melt material so a parameter equivalent to melting efficiency is not readily defined.

Nevertheless, it is interesting to note how efficiently a Friction Stir Welded sample uses the energy that it receives from the tool to make a weld. A higher energy utilization might be expected for FSW since lower temperatures (and hence less energy) are required than for fusion welding, and this temperature must be attained over the zone of stirred material which is roughly equivalent in size to a fusion weld melt zone. On the

other hand, Friction Stir Welds are always made against a relatively thick anvil plate which absorbs heat that would otherwise be available for reducing the flow stress of the work piece and facilitating the weld.

Using the above Figures for plasma welding of 6061 aluminum and assuming an arc efficiency of 50%, 540J/mm are delivered to the work piece to make the weld which is somewhat less than is needed to make the FSW weld. In this work, the anvil plate was low carbon steel, but higher weld efficiencies can probably be attained by using a lower thermal conductivity anvil plate such as stainless steel or a ceramic.

CONCLUSIONS

1. During Friction Stir Welding, three forces act on the work piece—a downward force, a longitudinal force in the direction of the weld, and transverse force in the ω x **v** direction.

Under typical welding conditions for 0.25 in. (6.35 mm.) thick 6061 aluminum (2mm/sec, .035 in plunge depth, 600 rpm rotational speed and 1° lead angle), a downward force of 2800 lbs. (12.5 kN), and longitudinal force of 300 lbs. (1.35 kN), and a transverse force of approximately 30 lbs. (135 N) are experienced in the ω x **v** direction.

For aluminum 2195 under typical weld conditions require a downward force of 3100 lbs., a longitudinal force of 920 lbs. (4.1 kN), and a transverse force of 45 lbs. (185 N) in the ω x **v** direction.

2. Friction Stir Welding is considerably more energy efficient than fusion welding made under similar conditions.

3. Adequate welds were made with downward forces as low as 2200 lbs. (10.5kN) and forces as high as 3100 lbs. (14.8 kN) did not cause excessive thinning of the welded section.

4. The transverse force changes direction when the direction of rotation of the pin tool is reversed. A model to account for the transverse force based on temperature and yield strength differences in the work piece at the front and the back of the pin tool is presented.

5. Since dynamic recrystallization takes place during the large deformations and high temperatures encountered in FSW, mechanical properties of material in the vicinity of the pin tool are not well known. Better property data is needed to be quantitative about the forces encountered during welding.

ACKNOWLEDGEMENT

The authors would like to acknowledge the generous support of NASA Marshall Space Flight Center under grant number NCC8-137. David Brown at UTEP gave much valuable assistance in experimental work.

REFERENCES

1. W. M. Thomas, *et al.*, Friction Stir Butt Welding. US patent, No. 5,460,317, 1991.
2. C. J. Dawes, "An Introduction to Friction Stir Welding and its Development", *Welding & Metal Fabrication.* Pp. 13-16, Jan., 1995
3. C. J. Dawes and W. M. Thomas, "Friction Stir Process Welds Aluminum Alloys", *Welding Journal,* Pp.41-45, March, 1996.
4. G. Liu, L. E. Murr, C. S. Niou, J. C. McClure and F. R. Vega, "Microstructural Aspects of the Friction-Stir Welding of 6061-T6 Aluminum", *Scripta Materialia.* Vol. 37, No. 3, Pp. 355-361, 1997.
5. O. T. Midling, "Material Flow Behavior and Microstructural Integrity of Friction Stir Butt Weldments", *Proceeding of 4th International Conference on Aluminum Alloys.* Atlanta, Ga., 1994.
6. H. G. Salem, A.P. Reynolds, J.S. Lyons, "Microstructure and Retention of Superplasticity in Friction Stir Welded Superplastic 2095 Sheet". *Scripta Materialia* Vol. 46, (2000), 337-342.
7. L. E. Murr, R.D. Flores, O.V. Flores, J.C. McClure, G. Liu, and D. Brown, "Friction-Stir Welding: Microstructural Characterization". *Mat. Res. Innovat.* No.1, Pp. 211-223, 1998.
8. L. E. Murr, G. Liu, and J. C. McClure, "A TEM Study of Precipitation and Related Microstructures in Friction-Stir Welded 6061 Aluminum", *Journal of Materials Science.* Vol. 33, Pp. 1243-1251, 1998.
9. Y. Sato, *et. al.* "Microtexture in the Friction-Stir Weld of an Aluminum Alloy". *Metallurgical and Materials Transactions*, Vol. 32A, April 2001, 941-948.

10. J. C. McClure, Z. Feng, W. Tang, J. E. Gould, L. E. Murr, and X. Guo, "A Thermal Model of Friction Stir Welding", *Proceedings 5th International Conference on Trends in Welding Research,* Pine Mountain, Georgia, June, 1998.

11. W. Tang, X. Guo, J.C. McClure, L. E. Murr, A. Nunes, "Heat Input and Temperature Distribution in Friction Stir Welding", to be published in *Journal of Materials Processing and Manufacturing Science.*

12. K. Colligan, "Material Flow Behavior during Friction Stir Welding of Aluminum" *Welding Journal*, 229-s-237-s, July, 1999.

13. Guerra, M., McClure, J.C., Murr, L. M., Nunes, A. C., "Material Motion During Friction Stir Welding", *Proceedings Friction Stir Welding and Processing*, Editor K.V. Jata, M.W. Mahoney, R.S. Mishra, TMS, 2001. TMS 2001, Indianapolis, Indiana, November 5-7, 2001.

14. T. U. Seidel, A.P. Reynolds, "Visualization of the Material Flow in AA2195 Friction-Stir Welds Using a Marker Insert Technique". *Metallurgical and Materials Transactions,* Vol. 32A, Nov. 2001, 2879-2884.

15. Mayerss, M., Chawla, K. *Mechanical Metallurgy*, Prentice Hall, Englewood Cliffs, N.J., p. 614, 1984.

16. *Handbook of Aluminum,* Alcan Aluminum Corporation, Third Edition, P. 64.

17. A. P. Reynolds and Wei Tang, "Alloy, Tool geometry, and Process Parameter Effects on Friction Stir Weld Energies and Resultant Joint Properties", *Proceedings of the Symposium on Friction Stir Welding and Processing.* p. 15-23, Eds. K. V. Jata, M. W. Mahoney, R. S. Mishura, S. L. Semiatin, and D. P. Field, TMS 2001, Indianapolis, Indiana, November 5-7, 2001.

18. *ASM Handbook Vol. 2. Properties and Selection: Nonferrous Alloys and Special-Purpose Materials.* ASM International, 1990.

19. M. Melendez, "Tool Stresses During Friction Stir Welding", Master's Thesis, University of Texas at El Paso, Metallurgical and Materials Engineering Department, 2002.

FIGURE CAPTIONS

Figure 1. Instrumented structure used to measure strain during FSW. (a) Side view of structure; (b) Top view of structure showing beam locations and high symmetry points A and B.

Figure 2. Schematic of one beam showing location of strain gauges.

Figure 3. Calibration of instrumented structure applying longitudinal, transverse and downward forces at points A and B.

Figure 4. Forces on work piece as a function of plunge depth. A weld in 6061 with no lead angle is also shown.

Figure 5. Schematic representing the probable origin of the transverse force. Arrows represent magnitude of the reactions at the front and back of the pin tool.

Figure 6. Downward forces for both alloys as a function plunge depth. A weld with no lead angle is also shown.

Figure 7. Longitudinal and transverse forces as a function of tool angular velocity.

Figure 8. Dynamically recrystallized zone (DRZ) width of 6061 at mid thickness as a function of tool angular velocity.

Figure 9. Downward force as a function of tool angular velocity.

Figure 10. Longitudinal and transverse forces as a function welding speed.

Figure 11. Downward force as a function of welding speed.

Figure 12. Forces on workpiece as a function of shoulder geometry. Three different shoulder configurations are shown in picture.

Figure 13. Longitudinal and transverse forces as a function of shoulder diameter.

Figure 14. Downward force as a function of shoulder diameter.

Figure 15. Specific weld energy for both alloys as a function of welding speed.

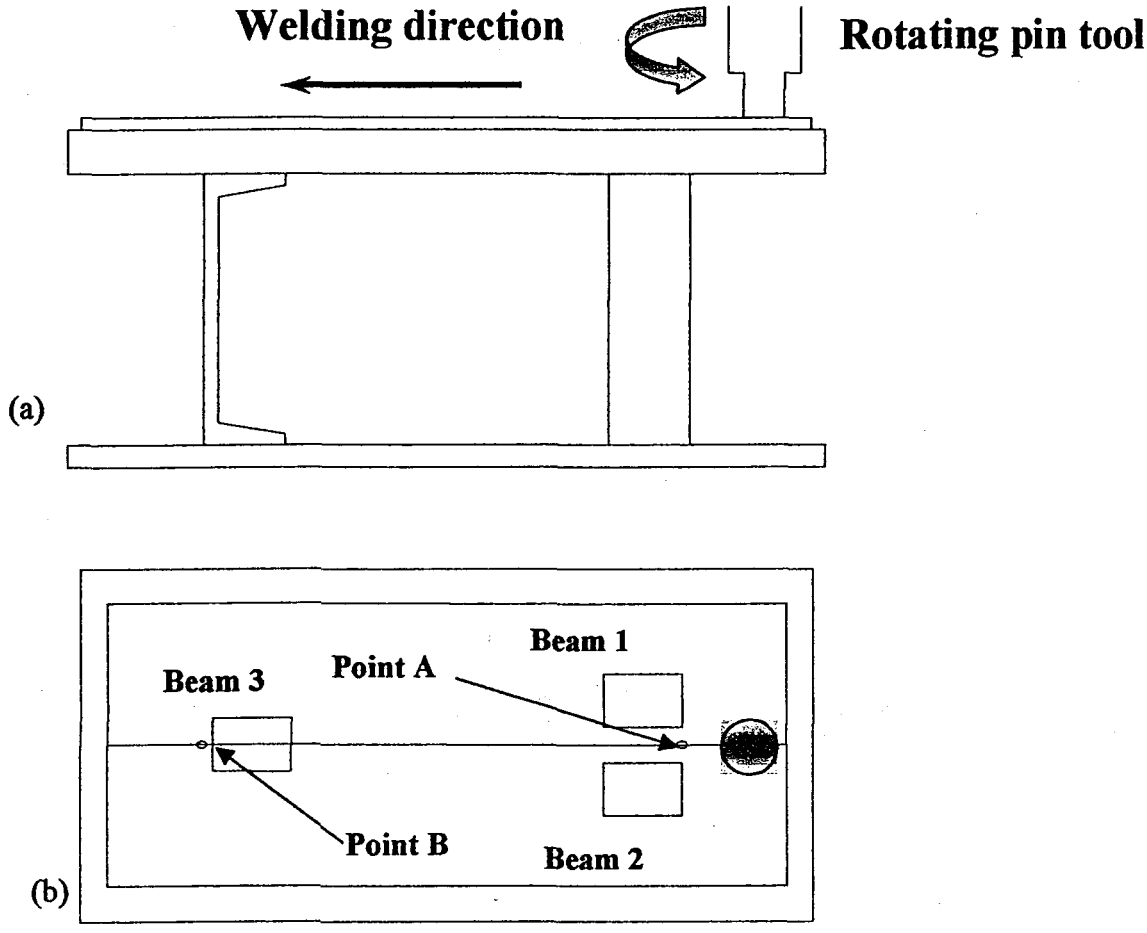

Figure 1

Melendez

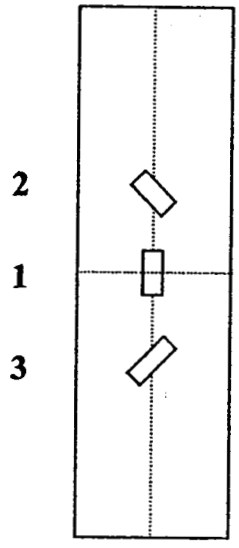

Figure 2

CALIBRATION

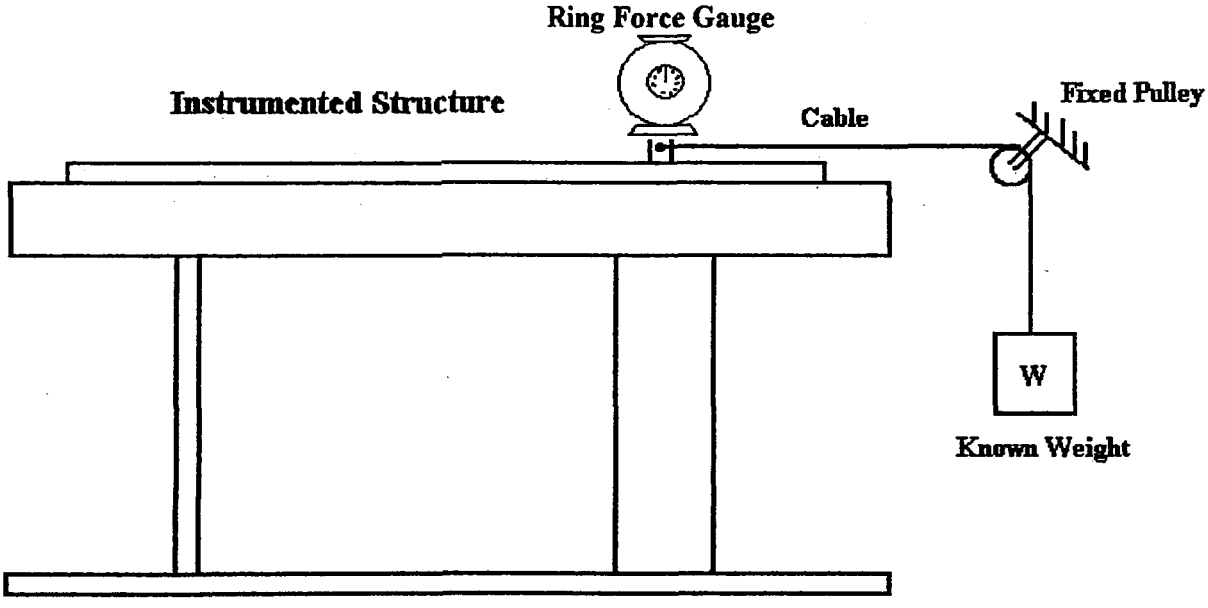

Figure 3

Melendez

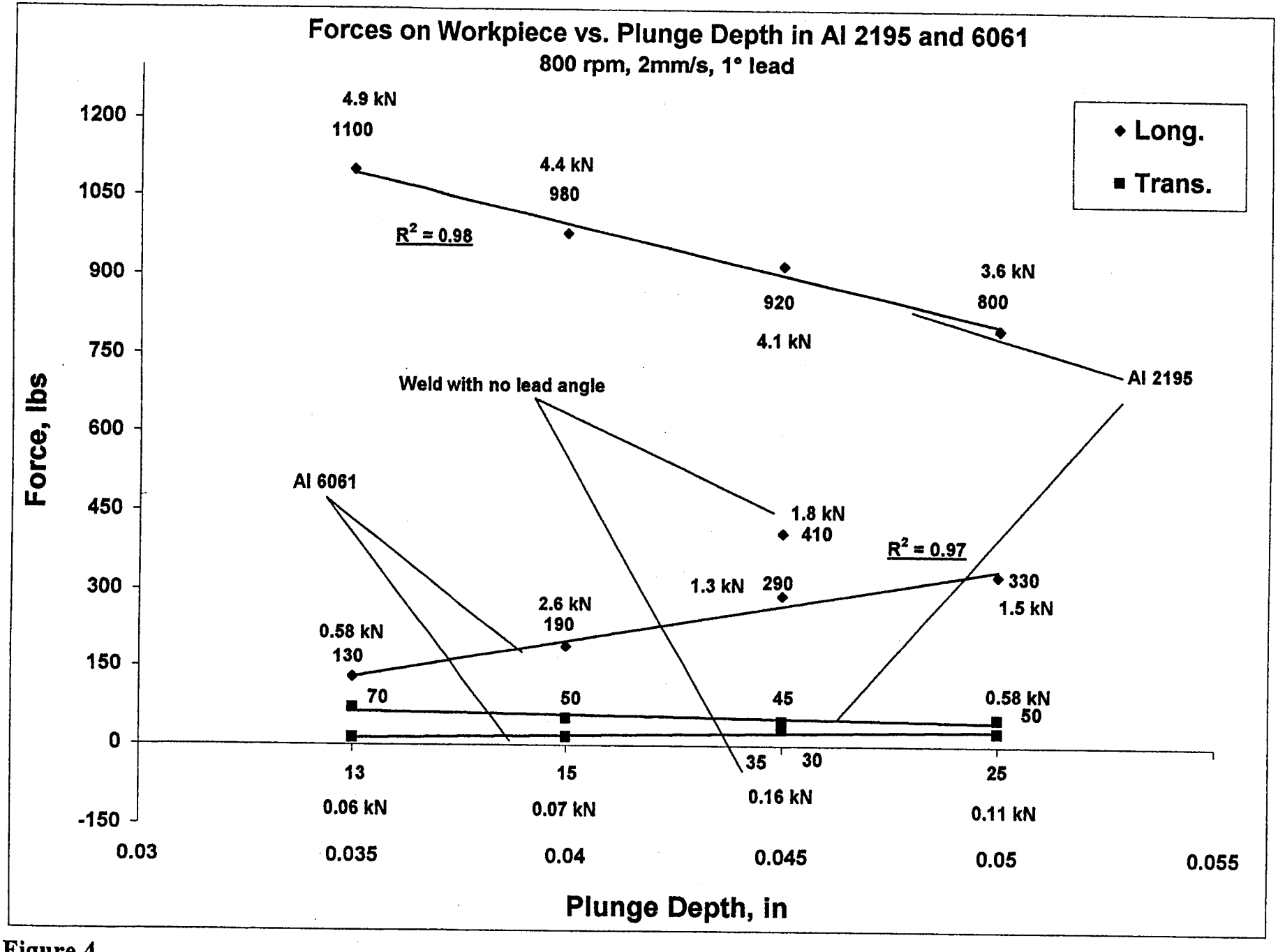
Forces on Workpiece vs. Plunge Depth in Al 2195 and 6061
800 rpm, 2mm/s, 1° lead
Long.
Trans.
Force, lbs
Plunge Depth, in
1200
1050
900
750
600
450
300
150
0
-150
0.03
0.035
0.04
0.045
0.05
0.055
4.9 kN
1100
4.4 kN
980
920
4.1 kN
3.6 kN
800
Al 2195
R² = 0.98
Weld with no lead angle
Al 6061
1.8 kN
410
R² = 0.97
1.3 kN
290
330
1.5 kN
2.6 kN
190
0.58 kN
130
70
50
45
0.58 kN
50
13
15
35
30
25
0.06 kN
0.07 kN
0.16 kN
0.11 kN

Figure 4

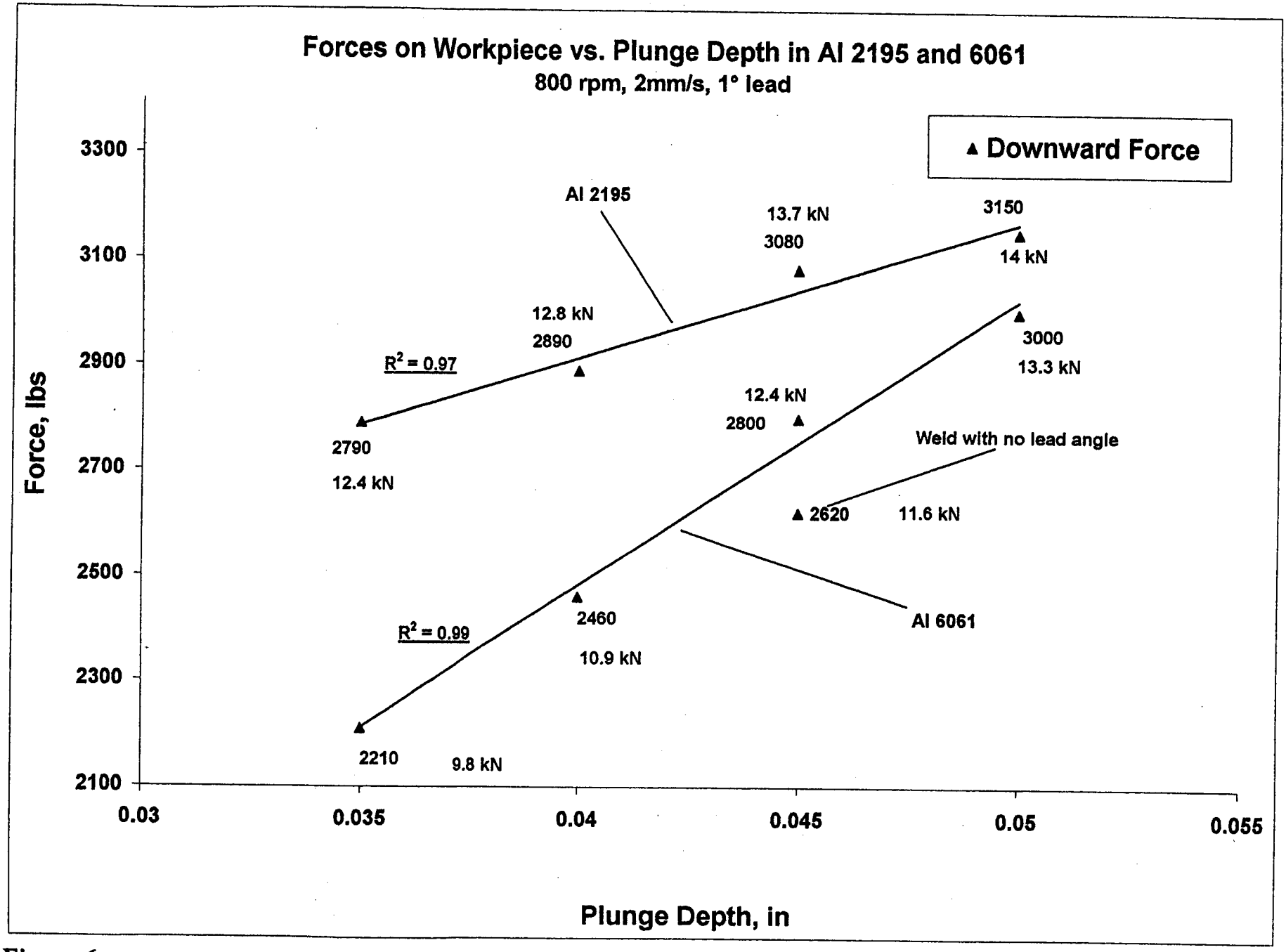
Forces on Workpiece vs. Plunge Depth in Al 2195 and 6061
800 rpm, 2mm/s, 1° lead
▲ Downward Force
Force, lbs
Plunge Depth, in
3300
3100
2900
2700
2500
2300
2100
0.03
0.035
0.04
0.045
0.05
0.055
Al 2195
13.7 kN
3080
3150
14 kN
12.8 kN
2890
R² = 0.97
3000
13.3 kN
12.4 kN
2800
2790
12.4 kN
Weld with no lead angle
2620
11.6 kN
2460
10.9 kN
Al 6061
R² = 0.99
2210
9.8 kN

Figure 6

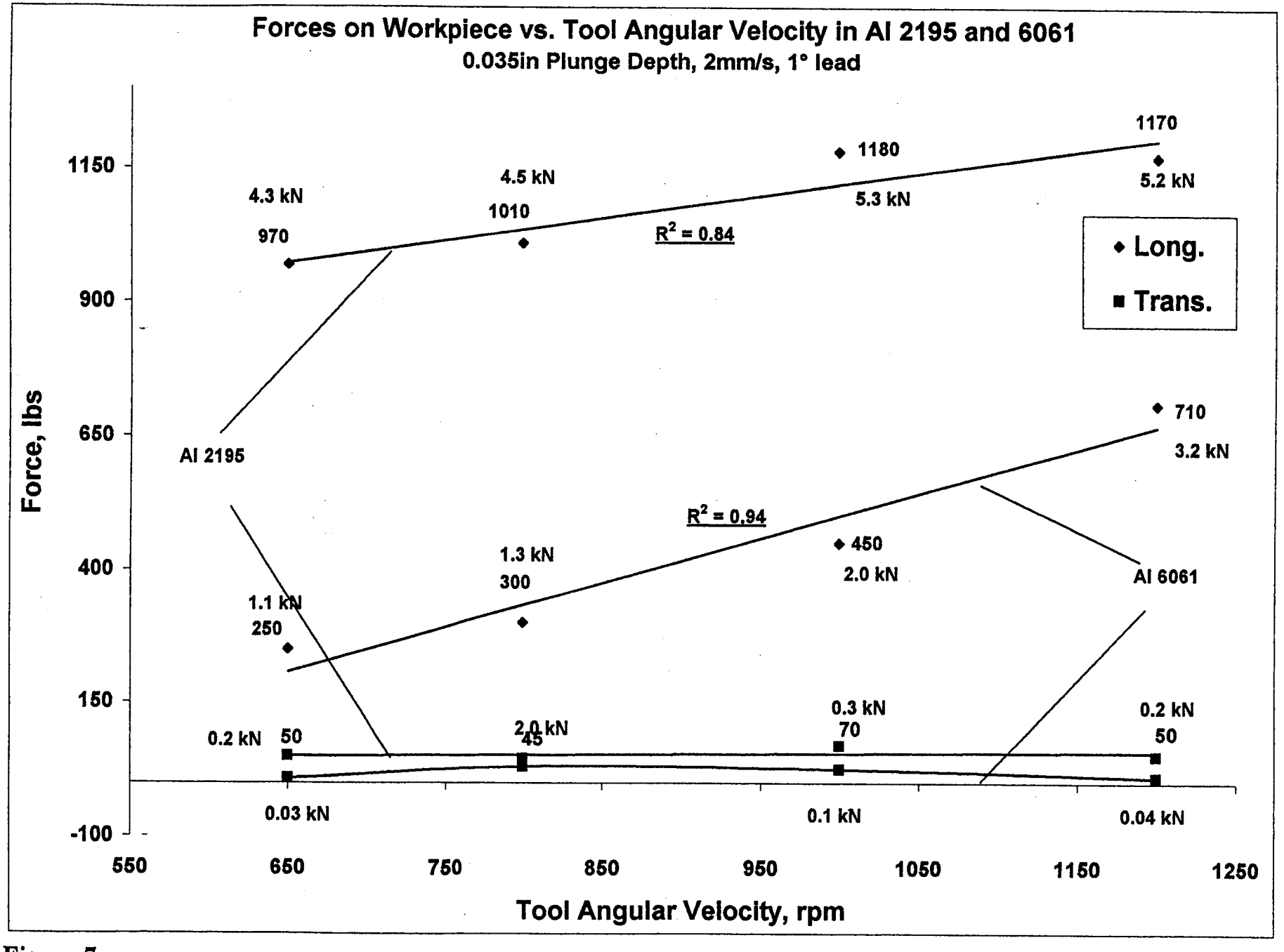
Forces on Workpiece vs. Tool Angular Velocity in Al 2195 and 6061
0.035in Plunge Depth, 2mm/s, 1° lead
Force, lbs
Tool Angular Velocity, rpm
1150
900
650
400
150
-100
550
650
750
850
950
1050
1150
1250
1170
1180
5.2 kN
4.5 kN
5.3 kN
4.3 kN
1010
970
R² = 0.84
Long.
Trans.
Al 2195
710
3.2 kN
R² = 0.94
1.3 kN
450
2.0 kN
Al 6061
300
1.1 kN
250
0.3 kN
0.2 kN
0.2 kN
2.0 kN
70
50
50
45
0.03 kN
0.1 kN
0.04 kN

Figure 7

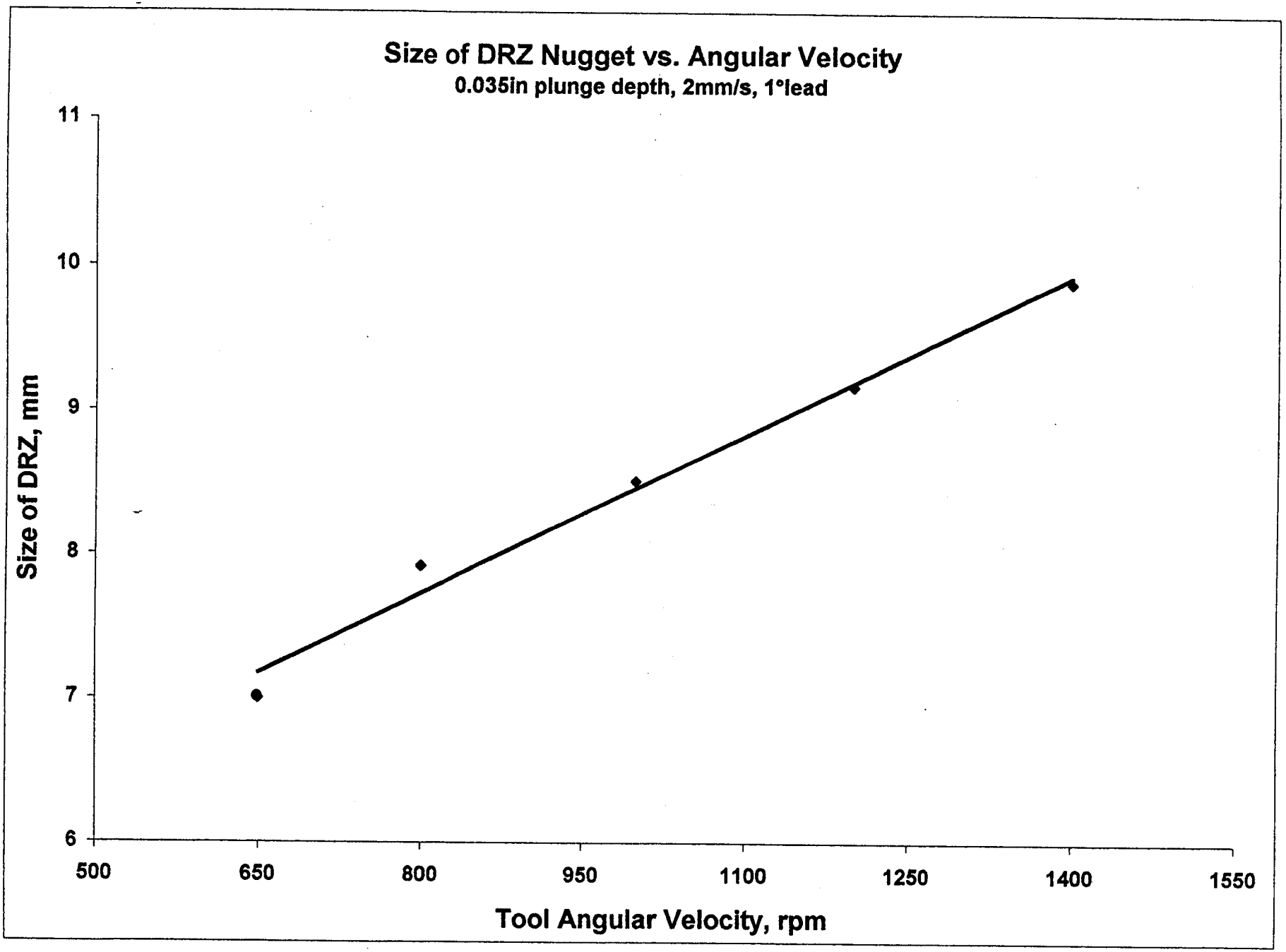
Size of DRZ Nugget vs. Angular Velocity
0.035in plunge depth, 2mm/s, 1°lead
Size of DRZ, mm
11
10
9
8
7
6
500
650
800
950
1100
1250
1400
1550
Tool Angular Velocity, rpm

Figure 8

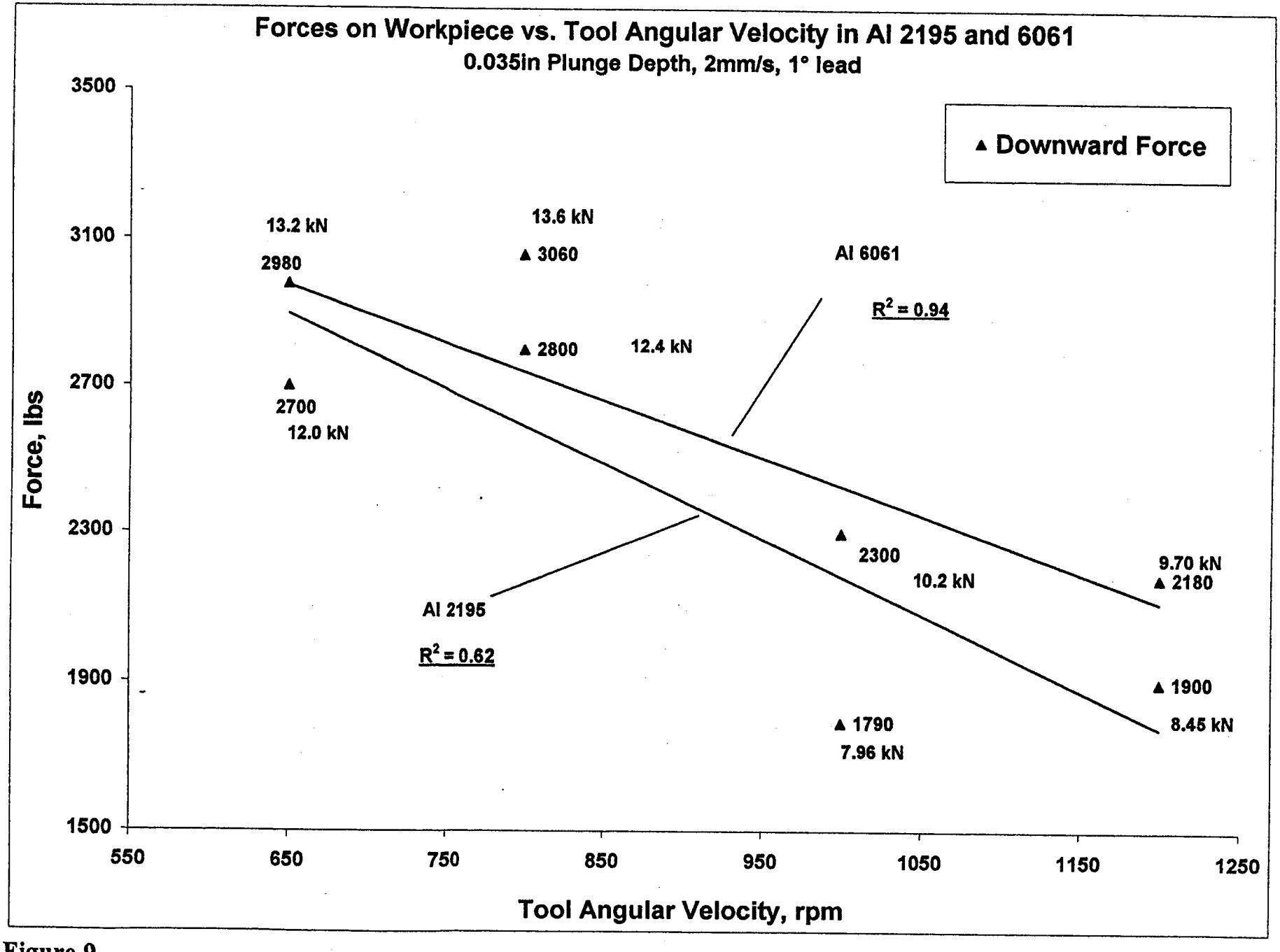
Forces on Workpiece vs. Tool Angular Velocity in Al 2195 and 6061
0.035in Plunge Depth, 2mm/s, 1° lead
▲ Downward Force
Force, lbs
3500
3100
2700
2300
1900
1500
550
650
750
850
950
1050
1150
1250
Tool Angular Velocity, rpm
13.2 kN
2980
13.6 kN
▲ 3060
Al 6061
R² = 0.94
▲ 2800
12.4 kN
▲ 2700
12.0 kN
▲ 2300
9.70 kN
▲ 2180
10.2 kN
Al 2195
R² = 0.62
▲ 1900
▲ 1790
7.96 kN
8.45 kN

Figure 9

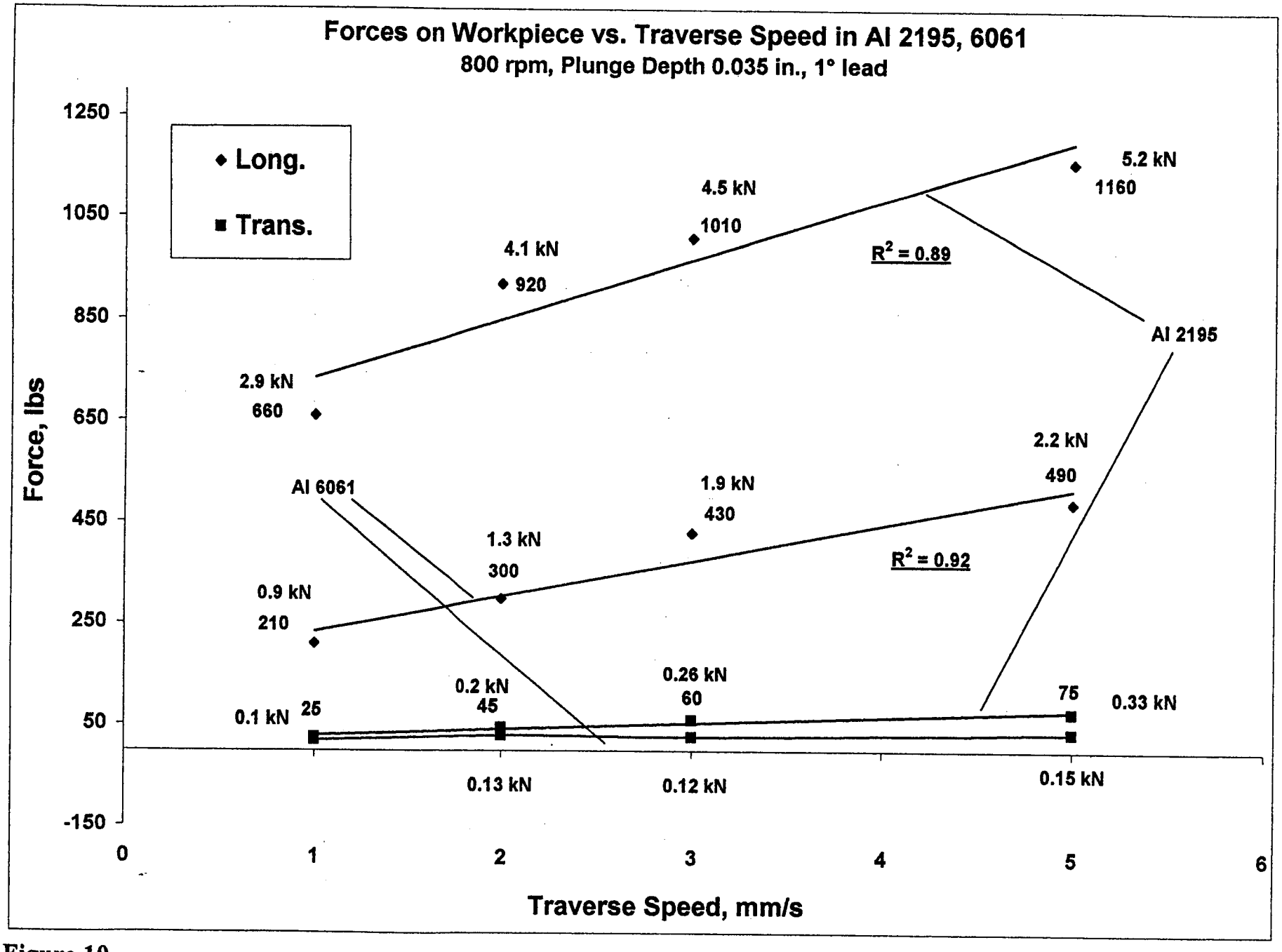
Forces on Workpiece vs. Traverse Speed in Al 2195, 6061
800 rpm, Plunge Depth 0.035 in., 1° lead
Long.
Trans.
Force, lbs
Traverse Speed, mm/s
1250
1050
850
650
450
250
50
-150
0
1
2
3
4
5
6
5.2 kN
1160
4.5 kN
1010
4.1 kN
920
2.9 kN
660
R² = 0.89
Al 2195
2.2 kN
490
1.9 kN
430
1.3 kN
300
0.9 kN
210
R² = 0.92
Al 6061
0.26 kN
60
0.2 kN
45
0.1 kN
25
75
0.33 kN
0.13 kN
0.12 kN
0.15 kN

Figure 10

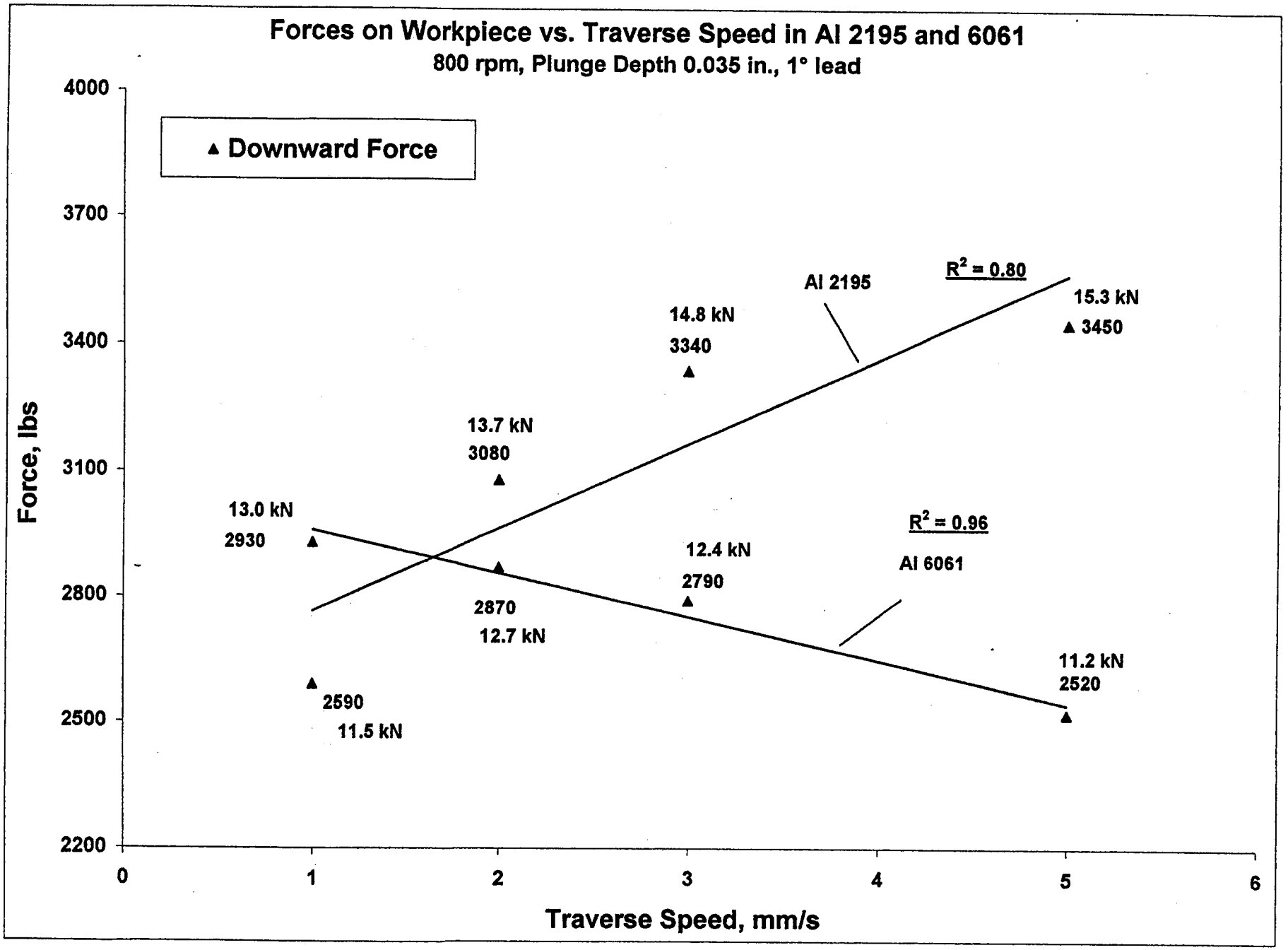
Forces on Workpiece vs. Traverse Speed in Al 2195 and 6061
800 rpm, Plunge Depth 0.035 in., 1° lead
▲ Downward Force
Force, lbs
Traverse Speed, mm/s
4000
3700
3400
3100
2800
2500
2200
0
1
2
3
4
5
6
Al 2195
R^2 = 0.80
15.3 kN
▲ 3450
14.8 kN
3340
13.7 kN
3080
13.0 kN
2930
2870
12.7 kN
2590
11.5 kN
R^2 = 0.96
Al 6061
12.4 kN
2790
11.2 kN
2520

Figure 11

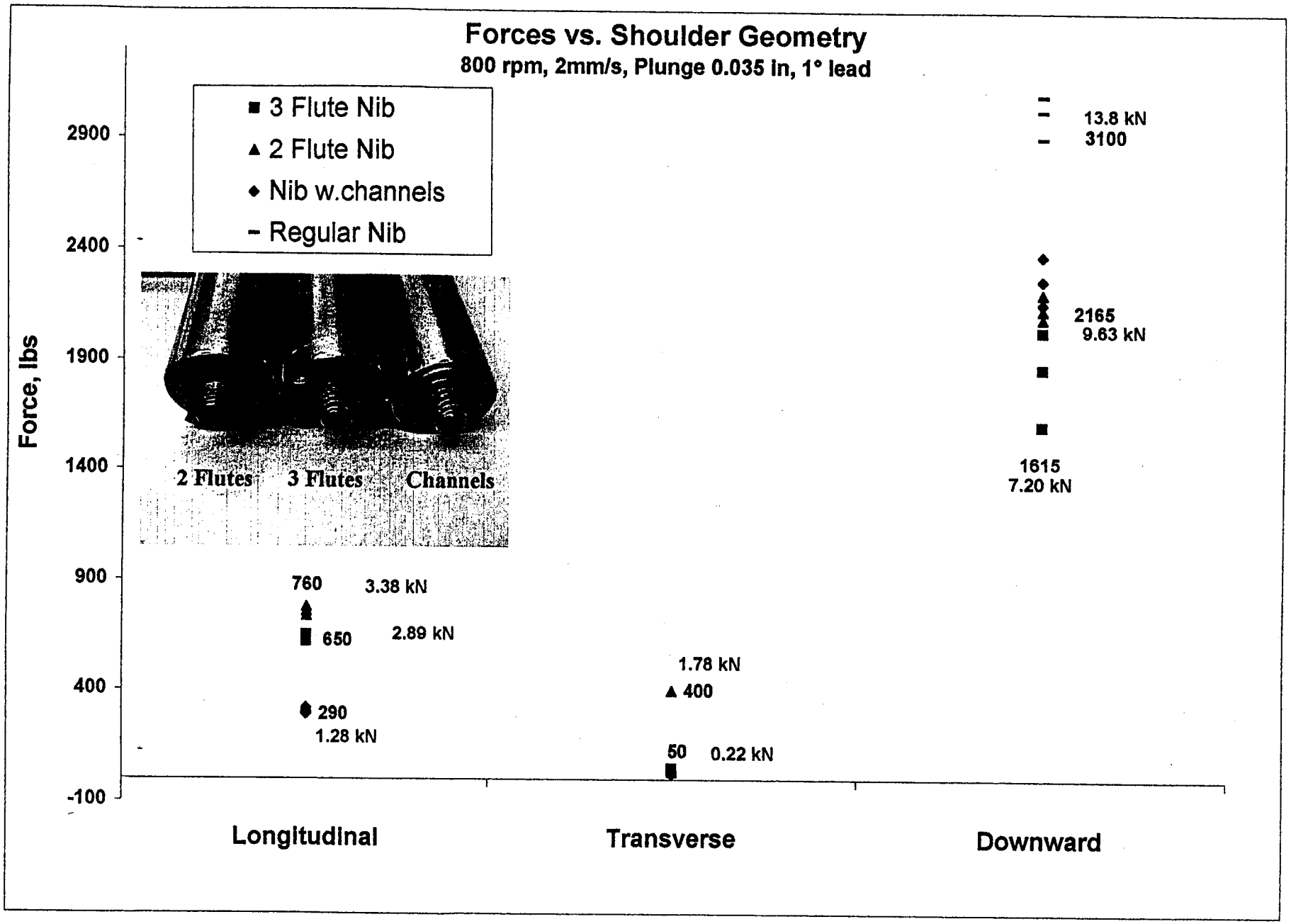
Forces vs. Shoulder Geometry
800 rpm, 2mm/s, Plunge 0.035 in, 1° lead
3 Flute Nib
2 Flute Nib
Nib w.channels
Regular Nib
Force, lbs
2900
2400
1900
1400
900
400
-100
2 Flutes
3 Flutes
Channels
760
3.38 kN
650
2.89 kN
290
1.28 kN
1.78 kN
400
50
0.22 kN
13.8 kN
3100
2165
9.63 kN
1615
7.20 kN
Longitudinal
Transverse
Downward

Figure 12

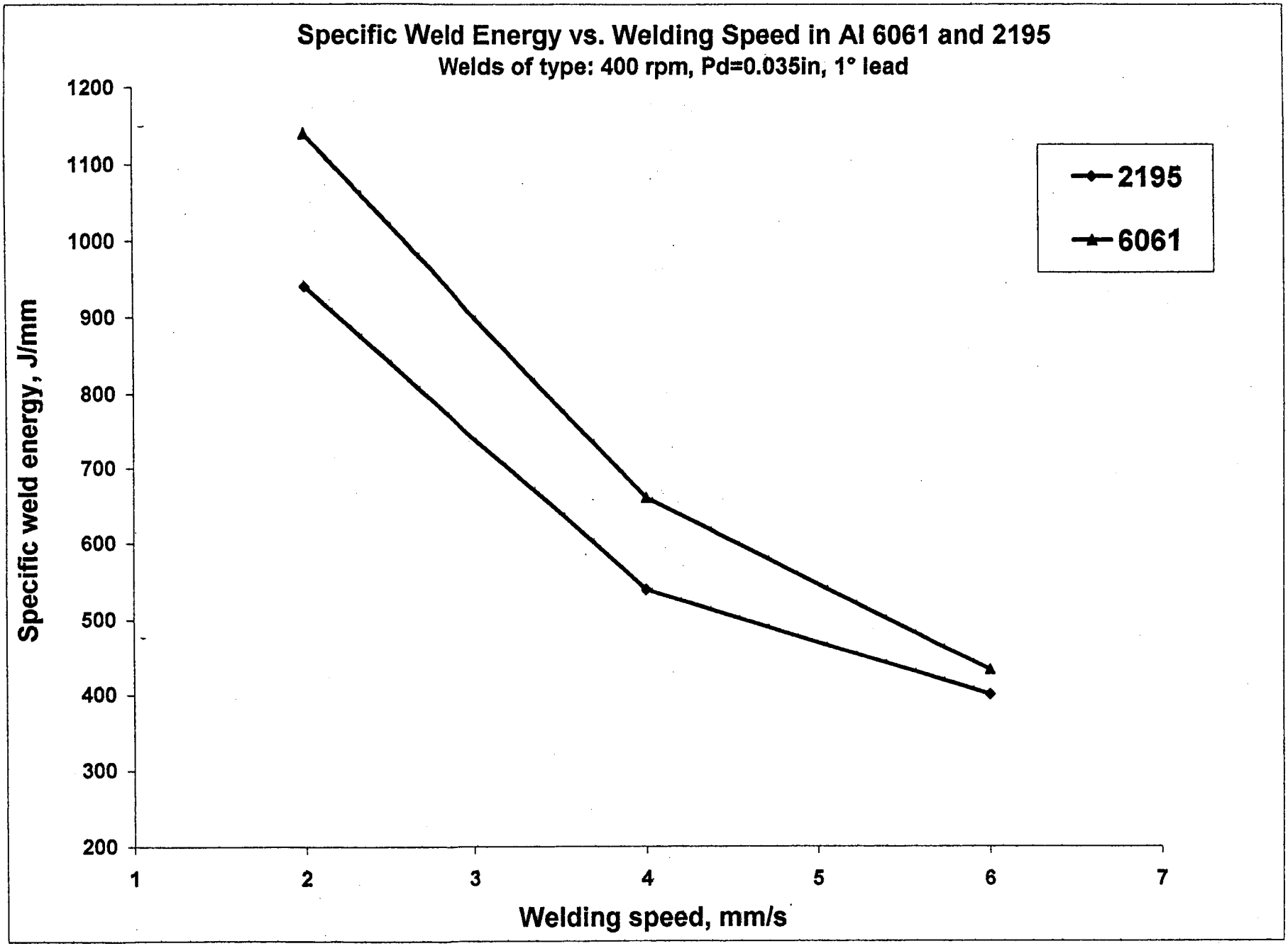
Specific Weld Energy vs. Welding Speed in Al 6061 and 2195
Welds of type: 400 rpm, Pd=0.035in, 1° lead
Specific weld energy, J/mm
1200
1100
1000
900
800
700
600
500
400
300
200
1
2
3
4
5
6
7
Welding speed, mm/s
2195
6061

Figure 15